

- 1946 (1966).
38. A. C. Neumann and I. Macintyre, in *Proceedings Fifth International Coral Reef Congress*, B. Delesalle, R. Galzin, B. Salvat, Eds. (Ant. Museum-Ephe, Moorea, French Polynesia, 1985), vol. 3, pp. 105–110.
 39. National Oceanic and Atmospheric Administration, *Bathymetric charts of Hawaii to Midway* (National Ocean Survey, U.S. Department of Commerce, Washington, DC, 1981).
 40. H. W. Menard, *Science* **220**, 913 (1983).
 41. B. U. Haq, J. Hardenbon, P. R. Vail, *ibid.* **235**, 1156 (1987).
 42. J. E. Hoffmeister and H. G. Multer, *Geol. Soc. Am. Bull.* **75**, 353 (1964).
 43. J. E. Bardach, *Science* **133**, 98 (1961).
 44. D. W. Kinsey, thesis, University of Hawaii, Honolulu (1979).
 45. L. Montaggione, *Ann. S. Afr. Mus.* **71**, 69 (1976).
 46. J. D. Milliman and K. O. Emery, *Science* **162**, 1121 (1968).
 47. K. J. Hsu and E. L. Winterer, *J. Geol. Soc. Lon.* **137**, 509 (1980).
 48. S. O. Schlanger, H. C. Jenkins, I. Premoli-Silva, *Earth Plan. Sci. Lett.* **52**, 435 (1981).
 49. D. Q. Bowen, *Nature* **238**, 621 (1980).
 50. J. I. Tracey, Jr., and H. S. Ladd, in *Proceedings of the Second International Coral Reef Symposium*, A. M. Cameron *et al.*, Eds. (Great Barrier Reef Committee, Brisbane, Australia, 1974), pp. 537–550.
 51. T. Spenser, *Coral Reefs* **4**, 59 (1985).
 52. J. F. Campbell, *Geo-Mar. Lett.* **6**, 139 (1986).
 53. T. A. Davies, P. Wilde, D. A. Clague, *Mar. Geol.* **13**, 311 (1972).
 54. B. Parsons and J. G. Sclater, *J. Geophys. Res.* **82**, 803 (1977).
 55. W. C. Pitman III, *Geol. Soc. Am. Bull.* **89**, 1389 (1978).
 56. We thank S. V. Smith, I. Macintyre, T. Jones, and J. Winterer for reading the manuscript and offering helpful suggestions. R.W.G. thanks the National Sea Grant Program (grant NA-81AA-D-00070) and the State of Hawaii, Office of Ocean Resources, Department of Business and Economic Development for financial support of this research. D.E. was supported by the Office of Naval Research and the National Science Foundation. Hawaii Institute of Marine Biology contribution No. 758, Department Business Economic Development contribution No. 72.

31 August 1988; accepted 22 December 1988

The Scanning Ion-Conductance Microscope

P. K. HANSMA, B. DRAKE, O. MARTI,* S. A. C. GOULD, C. B. PRATER

A scanning ion-conductance microscope (SICM) has been developed that can image the topography of nonconducting surfaces that are covered with electrolytes. The probe of the SICM is an electrolyte-filled micropipette. The flow of ions through the opening of the pipette is blocked at short distances between the probe and the surface, thus limiting the ion conductance. A feedback mechanism can be used to maintain a given conductance and in turn determine the distance to the surface. The SICM can also sample and image the local ion currents above the surfaces. To illustrate its potential for imaging ion currents through channels in membranes, a topographic image of a membrane filter with 0.80-micrometer pores and an image of the ion currents flowing through such pores are presented.

THE FAMILY OF SCANNING PROBE microscopes (1–4) is broadening the frontiers of surface imaging. These microscopes scan various sharp probes over samples to obtain surface contours—in some cases at the atomic scale (2). We report results from the SICM. It is designed specifically for biology and electrophysiology in that it can image soft nonconductors (such as membranes) that are covered with an electrolyte.

A schematic view of the SICM is shown in Fig. 1. A micropipette is filled with electrolyte and lowered through a reservoir of electrolyte toward an insulating sample surface while the conductance between an electrode inside the micropipette and an electrode in the reservoir is monitored. As the tip of the micropipette approaches the surface, the ion conductance decreases because the space through which ions can flow is decreased. The micropipette is then scanned laterally over the surface while a feedback system raises and lowers the micropipette to keep the conductance constant. The path of the tip follows the topography of the surface.

Preliminary experiments were performed in our lab in 1986 by J. Saad and G. Tarleton (5). They were able to measure the topography of machined plastic pieces using an eyedropper as a probe. These experiments were not pursued further because the scan ranges then available with our microscopes (6) were not much larger than the openings in available micropipettes.

However, x, y, z piezoelectric translators with larger scan ranges are now available,

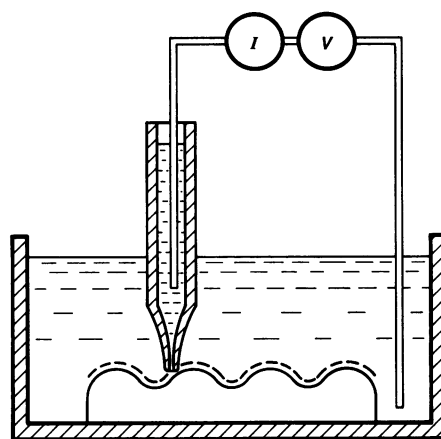


Fig. 1. The SICM scans a micropipette over the contours of a surface by keeping the electrical conductance through the tip of the micropipette constant by adjusting the vertical height of the probe.

and microscope design has evolved enough that experimentation with various scanning probes is relatively easy. The pipette of the SICM is brought near the surface with two fine screws that are adjusted by hand while the separation is monitored with an optical microscope (7). A third fine screw that is driven with a stepper motor (7) brings the pipette within range of a single-tube x, y, z piezoelectric translator (8). This translator has a 9.3- μm lateral range and a 3.0- μm vertical range (9).

The micropipettes for early experiments were made from 1.5-mm outer diameter (OD), 0.75-mm inner diameter (ID) Omega Dot (10) capillary tubing. Later versions were made with similar tubing (11) on a Brown-Flaming (12) puller. Although these pipettes are designed for measurement of intracellular potentials and patch clamping, similar micropipettes have been used in other scanning probe microscopes, namely the near-field scanning optical microscope and the micropipette molecule microscope (3). We estimated our micropipette tip diameters with a nondestructive bubble pressure method developed by Mittman *et al.* (13).

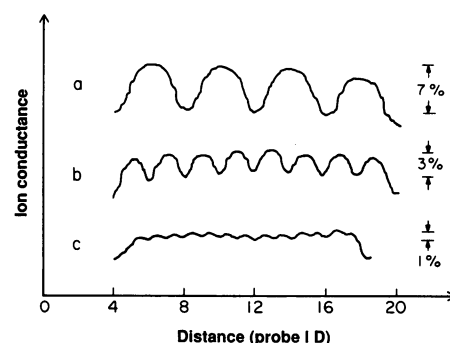


Fig. 2. Resolution test for the SICM. A pipette with an ID of 0.71 mm and an OD of 1.00 mm was scanned at constant height over three grooved plastic blocks with spacing of (a) four times, (b) two times, and (c) the same as the ID of the pipette. A 0.1M NaCl solution covered the blocks and filled the pipette. Note that even the grooves spaced by the ID of the pipette could be resolved.

Department of Physics, University of California, Santa Barbara, CA 93106.

*Present address: Institut für Quantenelektronik, ETH Hönggerberg, HPT, CH-8093 Zürich, Switzerland.

This method correlates the OD of the pipette to the internal pressure required for the pipette to produce a fine stream of bubbles in a liquid bath. The OD/ID ratio was essentially constant along the entire length of the pipette (14). Thus IDs were estimated from the OD/ID ratio of the unpulled capillary tubing. For the images we report the pipette tips had ODs of order 0.1 to 0.2 μm and IDs of order 0.05 to 0.1 μm .

Samples were glued onto glass substrates or directly onto electrodes (11) and then covered with a few drops of 0.1M NaCl. The micropipette tips were allowed to fill by capillary action with a commercial kit (10). The shafts were then backfilled with a syringe. In the pipettes we also used 0.1M NaCl to avoid concentration cell potentials and liquid junction potentials. Reversible Ag/AgCl microelectrode holders and bath electrodes (11) provided the necessary stability for reliable current and topographic imaging.

We applied dc voltages of 0.03 to 0.4 V to an electrode in the bath and measured dc currents (typically 1 to 10 nA) flowing into the pipette to determine the conductance, which was generally 10^{-8} to 10^{-7} S. The current was amplified by a preamplifier (preamp) used in a commercial scanning tunneling microscope (STM) (9). The preamp converted the current to a voltage with a 1 M Ω resistor, and the voltage was then amplified by a non-inverting amplifier with an AD544 operational amplifier with a voltage gain of 100. The overall current gain was 0.1 V/nA. We found it important to

mount the preamp directly on the microscope base to minimize stray capacitance and noise pickup. We operated the microscope with conductances 0.9 to 0.98 as great as the conductance when the tip was far from the surface. At smaller conductances the micropipette tip at times actually pressed into the sample surface.

We generated topographic images by measuring the voltage that the feedback system applied to the z -axis of the single-tube x,y,z translator to keep the conductance constant. For ion current images, the local current was monitored as the micropipette was scanned over the surface at a constant height z . A digital scanner supplied the x and y scan voltages for both topographic and ion-current images. The z values or ion currents together with their x and y coordinates were recorded on a video cassette recorder (VCR) with a digital data-acquisition system (15). The resulting image was filtered and shading or color scales were added to allow surface features to be more easily seen (16). The method of statistical differences (17), which enhances features on their local background while suppressing noise, was especially useful for processing current images.

The resolution of the SICM as a function of pipette diameter was measured with a large-scale model (Fig. 2). A glass pipette with an ID of 0.71 mm and an OD of 1.00 mm was scanned at a constant height over plastic blocks with regularly spaced grooves that were 0.71 mm deep. The height was set by lowering the pipette until the ion conductance decreased from 4.2×10^{-5} S, its

value when far from the surface, to 4×10^{-5} S. These conductances were measured at a frequency of 10 kHz. This resolution test showed that it should be possible, at least in principle, to resolve features as small as the ID of the micropipette if the noise on the ion conductance signal could be reduced to less than 1%.

In practice, we have resolved features a few times the ID of our micropipette, which was 0.05 to 0.1 μm . There is a compromise between averaging the ion-conductance signal for a long time to reduce noise and obtaining entire images in a reasonable time. We chose to acquire our images in ~ 5 min and found that the smallest resolvable features were of order 0.2 μm (Fig. 3).

The practical resolution limits of the SICM could be extended. As shown in Figs. 2 and 3, the SICM can resolve features on a scale set by the ID of the micropipette (although a large OD may prevent the tip from probing into a narrow, deep groove).

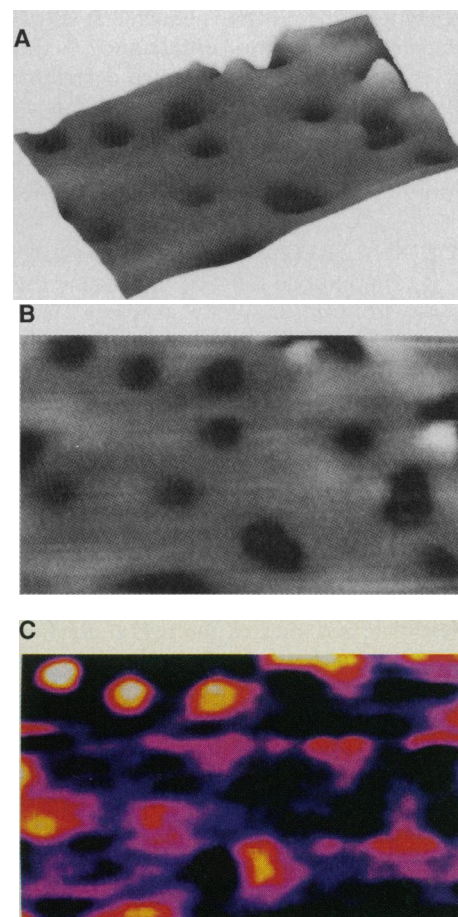
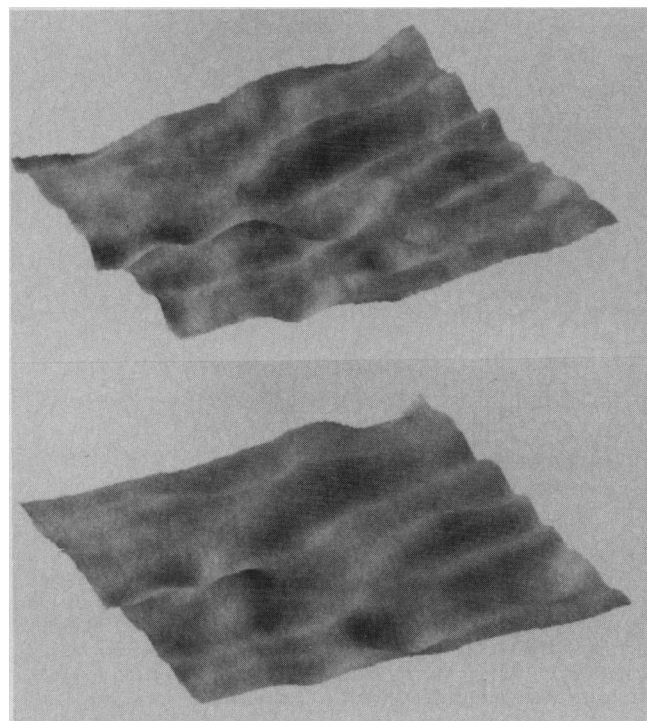


Fig. 3. These two SICM topographic images of the same area on an acetate film were taken a few minutes apart. The similarity of the images demonstrates that even soft samples are not damaged by the SICM. The imaged area is a square 4 μm on a side.

Fig. 4. (A) A SICM topographic image of the 0.8- μm diameter pores in a Nuclepore membrane filter (24). (B) The same image presented in a top view. (C) A SICM image of the ion currents coming out through the pores. The false colors go from black at the background level of current, 8 nA, up to white at the maximum level of ≈ 40 pA above the background. The imaged area is 7.8 μm by 4.5 μm for all three images.

Micropipettes with IDs as small as 30 nm have been produced for near-field scanning optical microscopes (18), and aluminosilicate pipettes with IDs of less than 10 nm have been made (19). The higher resistances of these smaller IDs should not be a problem; STMs have been operated with resistances thousands of times greater than our present values of 10 to 100 M Ω (20). The most serious limitation we have faced is that the smaller micropipette tips are extremely fragile and often break during a scan. Shorter taper pipettes may help with this problem and allow resolutions of 10 nm to be achieved.

The most promising application for the SICM is not, however, just imaging the topography of surfaces at submicrometer resolution. The SICM can image not only the topography, but also the local ion currents coming out through pores in a surface (Fig. 4). Comparison of topographic and ion current images can give a more detailed picture of the type of surface features that correlate with ion channels. In this model system, the comparison is simple: ion currents come through the holes as we would expect. Biological samples are more subtle, of course, as not every hole is an ion channel.

For images of the local ion currents, the micropipette was digitally scanned over the surface at a preselected height without movement in the z direction while the current flowing into the pipette at each point was measured (21). It was also possible to hold the micropipette over various locations on the imaged surface and measure local electrical properties. Thermal drift was small enough (~ 0.004 $\mu\text{m}/\text{min}$) that we could look, for example, at the time dependence of the ion currents above a pore, which was again simple for this model system (the current was constant), but which would be more subtle for biological samples.

The SICM offers both high-resolution topographic and ion-current images of non-conductors. Much of the necessary apparatus—micropipettes, microelectrodes, and current amplifiers—are already used routinely by electrophysiologists (19). Most of the positioning and feedback mechanism is the same as for the STM and is available commercially (22). Because the SICM operates in a saline solution or other ionic solutions, the microscope is well suited for biological applications. It complements the vibrating probe system (23) that can measure larger scale extracellular currents. An exciting extension of this work would be to use multiple-barrel micropipettes (10) with ion-specific electrodes (19). The total current into all of the barrels (or the current into one barrel with a nonspecific electrode)

could be used for feedback, while the microscope could simultaneously measure and image the flow of different ions. We anticipate that this technique can be used in the future by electrophysiologists to combine spatially resolved ion-flow measurements and topological imaging of biological membranes.

REFERENCES AND NOTES

1. For a review of scanning probe microscopes, see V. Martin, C. C. Williams, H. K. Wickramasinghe, *Scanning Microsc.* **2**, 3 (1988). Other scanning probe microscopes are described in (2–4).
2. Scanning tunneling microscope: G. Binnig, H. Rohrer, Ch. Gerber, E. Weibel, *Phys. Rev. Lett.* **49**, 57 (1982); atomic force microscope: G. Binnig, C. Quate, Ch. Gerber, *ibid.* **56**, 930 (1986).
3. Micropipette molecule microscope: J. A. Jarrell, J. G. King, J. W. Mills, *Science* **211**, 277 (1981); near-field scanning optical microscope: A. A. Lewis, M. Isaacson, A. Harootunian, A. Muray, *Ultramicroscopy* **13**, 227 (1984).
4. Scanning tunneling potentiometry: P. Murali and D. W. Pohl, *Appl. Phys. Lett.* **48**, 514 (1986); scanning electrochemical microscope: A. J. Bard, F. R. F. Fan, J. Kwak, O. Lev, *Anal. Chem.*, in press; scanning thermal profiler: C. C. Williams and H. K. Wickramasinghe, *Appl. Phys. Lett.* **49**, 1587 (1986); scanning capacitance microscope: J. R. Matey and J. Blanc, *J. Appl. Phys.* **57**, 1437 (1985).
5. J. Saad, G. Tarleton, P. K. Hansma, unpublished results.
6. B. Drake *et al.*, *Rev. Sci. Instrum.* **57**, 441 (1986).
7. B. Drake, R. Sonnenfeld, J. Schneir, P. K. Hansma, *Surf. Sci.* **181**, 92 (1987); W. J. Kaiser and R. C. Jaklevic, *ibid.*, p. 55.
8. G. Binnig and D. P. E. Smith, *Rev. Sci. Instrum.* **57**, 1688 (1986).
9. Digital Instruments, Santa Barbara, CA.
10. Frederick Haer & Co., Brunswick, ME.
11. World Precision Instruments, New Haven, CT.
12. Model P-77 from Sutter Instrument Company, San Rafael, CA.
13. S. Mittman, D. G. Flaming, D. R. Copenhagen, J. H. Belgum, *J. Neurosci. Methods* **22**, 161 (1987).
14. K. T. Brown and D. G. Flaming, *Neuroscience* **2**, 813 (1977).
15. This system had been previously used for an AFM and is described in more detail in O. Marti, S. Gould, P. K. Hansma, *Rev. Sci. Instrum.* **59**, 836 (1988).
16. Images were processed using a program developed at UCSB by O. Marti and S. A. C. Gould.
17. R. J. Wilson and S. Chiang, *J. Vac. Sci. Technol. A* **6**, 398 (1988); W. K. Pratt, *Digital Image Processing* (Wiley, New York, 1978), pp. 323–324.
18. E. Betzig *et al.*, *Proc. Soc. Photo-Opt. Instrum. Eng.* **897**, 91 (1988).
19. K. T. Brown and D. G. Flaming, *Advanced Micropipette Techniques for Cell Physiology* (Wiley, New York, 1986).
20. R. S. Becker *et al.*, *Nature* **325**, 419 (1987).
21. It is also possible to follow the topography with the ac ion current from one electrode in the bath and measure the dc ion currents from an electrode below the surface (or, perhaps, inside a cell).
22. For example, Park Instruments, Palo Alto, CA; Digital Instruments, Santa Barbara, CA; McAllister Technical Services, Berkeley, CA; Microscience Inc., Braintree, MA; and VG Instruments, Danvers, MA.
23. L. F. Jaffe, *Trends Neurosci.* **8**, 517 (1985).
24. Nuclepore Corporation, Pleasanton, CA.
25. We thank W. Stoeckenius and C. Bracker for suggesting that we image a Nuclepore filter; F. Haer for providing micropipettes and related equipment; E. Widder for help in making the later versions of the micropipettes; C. Bracker, J. Case, V. Elings, M. Haugan, E. Martzen, J. Saad, J. Schneir, G. Tarleton, and M. Wilson for their help; J. Belgum, C. Bessemer, K. Prater, C. Quate, and T. Sleator for useful discussions; K. Wickramasinghe and L. Inglehart for opening our eyes to the potential diversity of scanned probe microscopes; and G. Somorjai for pointing out the importance of studying liquid-solid interfaces. Supported in part by the Office of Naval Research (P.K.H., B.D., and O.M.) and by the Solid State Physics program in the Division of Materials Research of the National Science Foundation, under grant DMR8613486 (C.P., S.G., and P.K.H.).

6 October 1988; accepted 23 November 1988

A Diet-Induced Developmental Polymorphism in a Caterpillar

ERICK GREENE

Caterpillars of the spring brood of *Nemoria arizonaria* develop into mimics of the oak catkins upon which they feed. Caterpillars from the summer brood emerge after the catkins have fallen and they develop instead into mimics of oak twigs. This developmental polymorphism may be triggered by the concentration of defensive secondary compounds in the larval diet: all caterpillars raised on catkins, which are low in tannin, developed into catkin morphs; those raised on leaves, which are high in tannin, developed into twig morphs; most raised on artificial diets of catkins with elevated tannin concentrations developed into twig morphs.

MANY ORGANISMS OCCUR IN TWO or more distinct forms. Developmental polymorphisms (or polyphenisms) occur when phenotypic variation is produced by differences in environmental conditions rather than by differences in genetic constitution (1, 2). Such developmental polymorphisms are conspicuous among arthropods with life spans that are short relative to the scale of environmental varia-

tion: examples are some color forms of caterpillars, pupae, and butterflies (2), winged and nonwinged morphs of water striders (3) and planthoppers (4), sexual and asexual forms of aphids (5), and caste sys-

Department of Biology, Princeton University, Princeton, NJ 08544.

Present address: Department of Avian Sciences, University of California, Davis, CA 95616.